ANL-HEP-CP-78-52

CONF-780967--2

DIPROTON RESONANCES IN THE MASS REGION 2100 TO 2800 MeV

Akihiko Yokosawa

Meeting on Exotic Resonances
Hiroshima, Japan
September 1-2, 1978

U of C-AUA-USDOE

ARGONNE NATIONAL LABORATORY, ARGONNE, ILLINOIS

Operated under Contract W-31-109-Eng-38 for the
U. S. DEPARTMENT OF ENERGY

Meeting on Exotic Resonances
Hiroshima, Japan
September 1-2, 1978

Diproton Resonances in the Mass Region 2100 to 2800 MeV*

Akihiko Yokosawa

Argonne National Laboratory
Argonne, Illinois 60439

Abstract

A striking energy dependence has been observed in the difference between the p-p total cross sections for parallel and antiparallel longitudinal spin states, $\Delta\sigma_L = \sigma^{Tot}(\rightleftarrows) - \sigma^{Tot}(\rightrightarrows)$. The structure appears around p_{lab} = 1.5 GeV/c where $\Delta\sigma_L$ = -16.7 mb and is seen in $\sigma^{Tot}(\rightrightarrows)$ rather than $\sigma^{Tot}(\rightleftarrows)$. The experiments were performed at Argonne National Laboratory using a standard transmission technique.

From the dispersion analysis of a forward p-p scattering amplitude using the data on $\Delta\sigma_L$, Grein and Kroll have shown that the Argand plot of the amplitude has a clear resonance-like behavior around proton-incident momentum of 1.5 GeV/c. At the same energy range, the p-p polarization at fixed -t also shows a remarkable energy dependence. In addition, we have observed a prominent energy dependence for C_{LL}, the spin correlation parameter for elastic pp scattering with beam and target both longitudinally polarized. The possibility of a resonance was further pursued by studying Legendre expansion coefficients of p-p differential cross section and polarization data. The analysis showed a partial wave,

*Work supported by the U.S. Department of Energy.

$^3F_3$ consistent with having a resonant behavior. Based on a phase-shift analysis, Hoshizaki also showed that $^3F_3$ seems to resonate. This resonant state would have the quantum number $J^P = 3^-$, mass ∿2260 MeV, width ∿200 MeV and elasticity 20-30%. This exotic state may be described by the MIT bag model.

We also speculate several more diproton resonances in the mass region 2100 to 2800 MeV.

Introduction

We would like to start out by discussing the proton-proton total cross-section data at the intermediate-energy region. As shown in Fig. 1, up to 1.2-GeV/c incident proton momentum, the total cross section, which mainly consists of the elastic process, falls and then rises due to the inelastic-channel opening. The cross section flattens above 1.5 GeV/c. We observe no structures that may suggest the possible existence of a resonance.

However, we have observed totally unexpected structures in the total cross section when both the incident protons and target protons were longitudinally polarized. The most remarkable structure appears around p_{lab} = 1.5 GeV/c.

We mainly discuss the existence of at least one diproton resonance and its properties, and speculate three more such candidates. Such a resonance opens a new era in the nucleon-nucleon system and also is crucially important for further development of the quark models that require six quarks in a bag.[1-3]

First, we describe experimental observables in terms of the helicity amplitudes, and then in terms of singlet and triplet partial-wave amplitudes. There are three s-channel helicity amplitudes at $\theta_{c.m.} = 0$:

$$\phi_1 = \langle ++|++\rangle,$$
$$\phi_2 = \langle --|++\rangle, \text{ and}$$
$$\phi_3 = \langle +-|+-\rangle.$$

These amplitudes are related to total cross section as follows:

i) Spin averaged total cross section

$$\sigma^{Tot} = (2\pi/k)\,\mathrm{Im}\left\{\phi_1(0) + \phi_3(0)\right\} = (1/2)\left\{\sigma^{Tot}(\rightleftarrows) + \sigma^{Tot}(\rightrightarrows)\right\} \qquad (1)$$

ii) Difference between total cross sections for parallel and antiparallel spin states (longitudinal)

$$\Delta\sigma_L = (4\pi/k)\,\mathrm{Im}\left\{\phi_1(0) - \phi_3(0)\right\} = \left\{\sigma^{Tot}(\rightleftarrows) - \sigma^{Tot}(\rightrightarrows)\right\} \qquad (2)$$

iii) Difference between total cross sections for parallel and antiparallel spin states (transverse)

$$\Delta\sigma_T = -(4\pi/k)\,\mathrm{Im}\,\phi_2(0) = \sigma^{Tot}(\uparrow\downarrow) - \sigma^{Tot}(\uparrow\uparrow) \qquad (3)$$

Argonne ZGS facilities provide various spin directions of incident beam and target. Spin directions are illustrated below. To express observables in elastic scattering, we adopt the notation (Beam, Target; Scattered, Recoil); (0,N;0,0) for polarization, (N,N;0,0) and (L,L;0,0) for spin correlation parameters, etc. A typical experimental setup for $\Delta\sigma_L$ is shown in Fig. 2 (a). The measurements were done in standard transmission experiment.

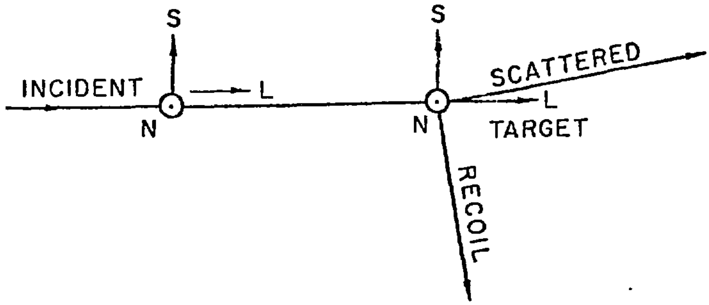

N: NORMAL TO THE SCATTERING PLANE
L: LONGITUDINAL DIRECTION
S = N x L IN THE SCATTERING PLANE

<u>$\Delta\sigma_L$ and $\Delta\sigma_T$ Measurements</u>

We show the results of $\Delta\sigma_L$ measurements from 1.0 to 6.0 GeV/c (Fig. 3a).[4-6] There is a sharp peak near 1.2 GeV/c and a dip near 1.5 GeV/c. From Eq. 2, a structure in $\phi_1(0)$ and $\phi_3(0)$ should appear as a peak and dip, respectively, in $\Delta\sigma_L$. Figure 3b shows $\sigma^{Tot}(\rightleftarrows)$ and $\sigma^{Tot}(\rightrightarrows)$ as obtained from Eqs. 1 and 2. There is a clear bump in $\sigma^{Tot}(\rightrightarrows)$. We observe the third structure in $\sigma^{Tot}(\rightleftarrows)$ near 2.0 GeV/c although that is not as remarkable as the one appearing in $\Delta\sigma_T$.

In Fig. 4, preliminary results of several $\Delta\sigma_L$ measurements up to 12 GeV/c are shown. (Several momentum points between 3 and 6 GeV/c have been measured, but they are not shown in the Figure.)

To study the behavior in terms of the partial scattering amplitudes, the data on $(k^2/4\pi)\Delta\sigma_L$ together with $(k^2/4\pi)\Delta\sigma_T$ are plotted in Fig. 5 as a function of the center-of-mass energy,[7] where k is the c.m. momentum. If the dip in $\Delta\sigma_L$ is considered to be due to a resonance, the mass is about 2260 MeV with a width of about 200 MeV. The 1.2-GeV/c peak is seen in $\Delta\sigma_L$ and possibly in $\Delta\sigma_T$ data. The 2.0-GeV/c peak is clearly visible in $\Delta\sigma_T$.

Using the data on $\Delta\sigma_L$, Grein and Kroll have calculated the real part of $\left[\phi_1(0) - \phi_3(0)\right]$ by applying dispersion relations.[8] In the Argand plot of the $\left[\phi_1(0) - \phi_3(0)\right]$ amplitude, we observe a clear resonance-like behavior around the incident proton momentum of 1.5 GeV/c (mass $\approx$ 2260 MeV) and possibly at 1.2 GeV/c (mass $\approx$ 2100 MeV) as shown in Fig. 6.

When the helicity amplitudes are decomposed into partial waves,[9]

$$\mathrm{Im}\phi_1(0) = \frac{1}{k} \sum_J \mathrm{Im}\left\{ (2J+1)R_J + (J+1)R_{J+1,J} + JR_{J-1,J} + 2\left[J(J+1)\right]^{\frac{1}{2}} R^J \right\}, \quad (4)$$

$$\mathrm{Im}\phi_2(0) = \frac{1}{k} \sum_J \mathrm{Im}\left\{ -(2J+1)R_J + (J+1)R_{J+1,J} + JR_{J-1,J} + 2\left[J(J+1)\right]^{\frac{1}{2}} R^J \right\}, \quad (5)$$

and

$$\mathrm{Im}\phi_3(0) = \frac{1}{k} \sum_J \mathrm{Im}\left\{ (2J+1)R_{JJ} + JR_{J+1,J} + (J+1)R_{J-1,J} - 2\left[J(J+1)\right]^{\frac{1}{2}} R^J \right\}, \quad (6)$$

where R_J is the spin-singlet partial-wave amplitudes with J = L = even, R_{JJ} and $R_{J\pm1,J}$ are spin-triplet waves with J = L = odd and $J = L \mp 1$ = even, respectively, and R^J is the mixing term. The partial wave characteristics to $\phi_1(0)$ is R_J and to $\phi_3(0)$ is R_{JJ}; the peak in Fig. 3a is due to one of the singlets $^1S_0$, $^1D_2$,..., and the dip is due to one of the triplets $^3P_1$, $^3F_3$,... .

Structure in σ_{el}^{Tot} and Polarization

So far, such a behavior is discussed only at $|t| = 0$, and the properties of the possible resonance (e.g., spin and parity) are not determined. One needs to study the angular distributions of the observables in pp scattering. Let us see if we observe a similar structure in other channels. Figure 7 shows the elastic total cross section, σ_{el}^{Tot}.[10,11] There is also a structure in the plot of polarization against incident momentum at fixed $|t|$, as shown in Fig. 8.[12] We note that the structure in polarization has nothing to do with the peak in $\Delta\sigma_L$ at 1.2 GeV/c, because the polarization does not include singlet terms.

Legendre Coefficient Analysis

We pursue the possibility of the existence of such a resonance and investigate the nature of the possible resonance by studying differential cross-section and polarization data in pp elastic scattering around 1.5 GeV/c. Our interest then is to investigate if an R_{JJ} partial wave has the behavior of a Breit-Wigner formula. The effect of resonances can be studied through the energy dependence of the Legendre expansion coefficients obtained from the differential cross-section and polarization data.[11,12] We report the results of such an analysis using data at 1.0 - 2.0 GeV/c.[9] The analysis was carried out by looking at the energy dependence of the coefficients a_n and b_n in the expansions:

$$d\sigma/d\Omega = \lambda\!\!\!^{-2} \sum_{n=0}^{N} a_n P_n(\cos\theta) \tag{7}$$

$$P d\sigma/d\Omega = \lambda\!\!\!^{-2} \sum_{n=2}^{N} b_n P_n^{(1)}(\cos\theta) \tag{8}$$

These coefficients are related to various partial waves, and we show only relevant relations here.

The coefficients a_n, obtained by fitting differential cross-section data to Eq. 7, mainly tell us that the highest significant value of J is four; a_8 and higher coefficients are nearly zero, and we ignore those terms with $J > 4$ and $L > 4$. Figure 9 shows the coefficients b_n obtained by fitting the product of differential cross-section and polarization data, plotted against incident momentum and energy. All coefficients up to and including b_6 have a remarkable energy dependence around $p_{lab} \approx 1.5$ GeV/c. We need to know if such a rapid change is due to one or two resonant partial waves while the other amplitudes vary slowly with energy; our particular attention is on the R_{JJ} partial waves, $^3P_1$ and $^3F_3$. We determine how the behavior compares with the Breit-Wigner formula,

$$A_{res} = (\varepsilon + i)\ (\Gamma_{el}/\Gamma)/(\varepsilon^2 + 1),\ \text{where}\ \varepsilon = 2(E_o - E)/\Gamma \qquad (9)$$

The energy dependence of this formula is illustrated in Fig. 9.

In general, the coefficient with higher order is easier to interpret because fewer terms are involved. The coefficient b_6 is related to the partial-wave amplitude by

$$b_6 = 1.8\ (\mathrm{Im}\,^3F_3\mathrm{Re}\,^3F_4 - \mathrm{Re}\,^3F_3\mathrm{Im}\,^3F_4) + \ldots, \qquad (10)$$

where residual terms (...) include neither $^3F_3$ nor $^3P_1$. A rise in b_6 with respect to energy is consistent with $^3F_3$ following the Breit-Wigner formula while other amplitudes vary slowly with energy; the value of the first term in Eq. 10 is the same both before and after resonance, say at 2110 and 2410 MeV, respectively, and the difference in b_6 at these energies is due to the second term, which has $-\mathrm{Re}A_{res}$ changing from minus to plus ($\mathrm{Im}\,^3F_4 > 0$ by unitarity). We note that $^3P_1$, another possible resonance candidate in R_{JJ}, is absent in b_6. Other coefficients are also consistent with the interpretation.

C_{LL} = (L,L;0,0) Measurements

Simultaneously with $\Delta\sigma_L$ measurements, we have measured the spin-spin correlation parameter $C_{LL}(\theta_{c.m.}) = (L,L;0,0)$ in p-p elastic scattering for $70^\circ \leq \theta_{c.m.} \leq 110^\circ$ at p_{lab} = 1.0 to 3.0 GeV/c.[13] A typical experimental setup is shown in Fig. 2(b).

The differential cross section for a particular spin direction of beam and target, $I^{\pm\pm}$, is given by

$$I^{\pm\pm}(\theta_{c.m.}) = I_o(\theta_{c.m.}) \left[1 + (\pm P_B)(\pm P_T) C_{LL}(\theta_{c.m.})\right], \tag{11}$$

where P_B and P_T are the beam and target polarization respectively, and + (-) refers to the spin state parallel (antiparallel) to the L direction (beam direction); $I_o(\theta_{c.m.})$ is the spin-averaged differential cross section. The parameter $C_{LL}(\theta_{c.m.})$ is then found to be

$$C_{LL}(\theta_{c.m.}) = \frac{1}{P_B P_T} \frac{(I^{++} + I^{--}) - (I^{+-} + I^{-+})}{(I^{++} + I^{--}) + (I^{+-} + I^{-+})}. \tag{12}$$

Figure 10 shows the angular dependence observed for the parameter C_{LL} at various incident-beam momenta. The errors shown are purely statistical, which dominate over systematic errors. The values of C_{LL} are all positive over the range covered, and are consistent with a symmetry about $\theta_{c.m.} = 90^\circ$ as expected for scattering of identical particles. Figure 10 also shows the predicted curves from existing phase-shift solutions.[14]

The values of C_{LL} at $\theta_{c.m.} = 90^\circ$ are plotted with respect to the incident momenta as shown in Fig. 11. We observe a sharp dip near p_{lab}=

1.2 GeV/c, rapid decrease near 1.5 GeV/c, and additional structure near p_{lab} = 2.0 GeV/c. A way to study these structures is to define C_{LL} in terms of partial wave amplitudes. Using the s-channel helicity amplitudes $\phi_1 = \langle ++|\phi|++\rangle$, $\phi_2 = \langle --|\phi|++\rangle$, $\phi_3 = \langle +-|\phi|+-\rangle$, $\phi_4 = \langle +-|\phi|-+\rangle$, and $\phi_5 = \langle ++|\phi|+-\rangle$, we have

$$C_{LL}\ (d\sigma/d\Omega) = \tfrac{1}{2}\left[-|\phi_1|^2 - |\phi_2|^2 + |\phi_3|^2 + |\phi_4|^2\right], \qquad (13)$$

where $d\sigma/d\Omega = \frac{1}{2}\left[|\phi_1|^2 + |\phi_2|^2 + |\phi_3|^2 + |\phi_4|^2 + 4|\phi_5|^2\right]$ is the spin-averaged differential cross section.

The amplitudes ϕ_1 through ϕ_5 are then expanded in terms of partial wave amplitudes. The spin-singlet partial waves, $^1S_0$, $^1D_2$, $^1G_4$..., appear in ϕ_1 and ϕ_2 with opposite signs, and the spin-triplet partial waves with L = J = odd, $^3P_1$, $^3F_3$,..., appear in ϕ_3 and ϕ_4 with opposite signs.

Figure 12a shows the quantity on $k^2\ C_{LL}\ (d\sigma/d\Omega)$ at $\theta_{c.m.} = 90^o$ plotted with respect to the incident momenta.[15] This quality is dimensionless and allows us to study the contributions of partial waves more directly.

First we examine if the rapid decrease observed in Figs. 11 and 12a near p_{lab} = 1.5 GeV/c is consistent with the partial wave $^3F_3$ having a resonant behavior.[9] Eq. 13 can be expressed in terms of $^3F_3$ and interfering partial waves as

$$\left[k^2 C_{LL}(d\sigma/d\Omega)\right]_{90^o} = \left[0.77\ |^3F_3|^2 + a(\mathrm{Re}\,^3F_3) + b(\mathrm{Im}\,^3F_3) + \ldots\right], \qquad (14)$$

where a (b) is the real (imaginary) part of the sum of other partial waves and the values can be estimated from the results of a phase-shift analysis.[14] By substituting these values and the $^3F_3$ resonance at mass = 2260 MeV with a width = 200 MeV and elasticity = 0.2 into Eq. 14, we find the same amount of rapid decrease as shown in Fig. 12a.

Next, we discuss the structure around p_{lab} = 2 GeV/c in Fig. 12a From the resonant-like structure in $(k^2/4\pi)\Delta\sigma_T$ as shown in Fig. 5, we expect it is due to a singlet spin state.[6,7] The contribution of spin singlet waves to Eq. 13 is

$$k^2 C_{LL}(d\sigma/d\Omega) = -|{}^1S_0 + 5\ {}^1D_2 P_2(\cos\theta) + 9\,{}^1G_4 P_4(\cos\theta) + \ldots|^2 + \ldots, \quad (15)$$

in which the contribution of ${}^1G_4$ vanishes at $\theta \approx 70^\circ$, where $P_4 = 0$.

The structure around 2 GeV/c is absent in Fig. 12(b), where the values of $k^2 C_{LL}\ d\sigma/d\Omega$ at $\theta_{c.m.} = 70^\circ$ are plotted as a function of beam momentum. Thus we may conclude that ${}^1G_4$ wave is responsible for the structure.[16]

Next, we discuss the sharp dip observed at 1.17 GeV/c as shown in Figs. 12a and 12b. We consider this due to a spin-singlet wave, because structures also appear as a peak both in $\Delta\sigma_L$ and $\Delta\sigma_T$.[6,7] In particular, we suspect they are due to the ${}^1D_2$ wave, because it is the only wave that couples to the s wave NΔ state, which is responsible for the rapid increase of pp total cross section near 1.2 GeV/c. We also point out that a resonance-like bump was observed in the cross-section of $pp \rightarrow \pi d$ in the same energy range,[17] which is usually interpreted in terms of the final-state interaction between one of the nucleons and π, forming Δ(1236) in the intermediate state.

The dip structure in Figs. 12a and 12b may come from the resonant-like behavior of the ${}^1D_2$ state.[14,18,19]

We conclude that the measurement of the spin-spin correlation parameter C_{LL} in pp elastic scattering near $\theta_{c.m.} = 90^o$ has revealed rich structure in $p_{lab} = 1.0 - 3.0$ GeV/c, which is consistent with the presence of $^3F_3$, and possibly $^1G_4$ and $^1D_2$ resonances.

C_{NN} = (N,N;0,0) Measurements at $\theta_{c.m.} = 90^o$

The measurement of the spin-spin correlation parameter C_{NN} in pp elastic scattering at $\theta_{c.m.} = 90^o$ also reveal a strong energy dependence. A plot of $k^2C_{NN}(d\sigma/d\Omega)$ in the momentum region 1 to 6 GeV/c is shown in Fig. 13.[20,21] We find that the energy dependence is consistent with the existence of $^1D_2$ and $^3F_3$ resonances.

Real Part of Scattering Amplitude at $|t| = 0$

The real part of scattering amplitude in the forward region in pp elastic scattering has been experimentally determined.[22] A plot of Re/Im at $|t| = 0$ is shown in Fig. 14. The real part changes from positive to negative as energy increases and becomes zero at around 1.5 GeV/c. The behavior is consistent with the existence of $^1D_2$ and $^3F_3$ resonances.[14]

Any Other Structure?

Do we observe any structure above a mass of 2500 MeV? Measurements of $\Delta\sigma_L$ and $\Delta\sigma_T$ are yet to be made at small-momentum interval. But we observe a remarkable energy dependence in C_{NN} = (N,N;0,0) data at all angles[23] and also at $\theta_{c.m.} = 90^o$.[21] As shown in Fig. 10 C_{LL} = (L,L;0,0) data are all positive at large angle up to 3.0 GeV/c, but we observe negative values as large as -35% at 6 GeV/c.[24]

Theoretical Models Without Resonances

There are several attempts to explain the structure in $\Delta\sigma_L$ data by Deck models,[25] by opening of inelastic channels, etc.[26,27] So far, none of the models explained the structure at 1.5 GeV/c.

Conclusion

A summary of diproton resonances is given in Table I. The name, B^2, of resonances was adopted during the Tokyo conference.

Table I

Diproton Resonances

Name	$B^2(2.14)$	$B^2(2.22)$	$B^2(2.43)$
Mass, GeV	2.14 - 2.17	2.20 - 2.26	2.43 - 2.50
I	1	1	1
Width, MeV	50-100	100-150	∿150
Elasticity	∿0.1	∿0.2	
pp State	$^1D_2$	$^3F_3$	$^1S_0$ or $^1G_4$
Remarks	$\Delta\sigma_L$, $\Delta\sigma_T$, C_{LL} Arndt et al. Hoshizaki	$\Delta\sigma_L$, P, C_{LL} Hidaka et al. Hoshizaki	$\Delta\sigma_T$, C_{LL} Hoshizaki

We are aware that the structure in $\Delta\sigma_L$ around 1.5 GeV/c consists of both singlet and triplet spin states. As shown in Fig. 5, $\Delta\sigma_T$ data contain only singlet structures. Then we expect to see only the triplet structure in $(\Delta\sigma_T - \Delta\sigma_L)$ as shown in Fig. 15. In this case the mass of $B^2(2.22)$ would be somewhat higher.

<u>Present Status of $\Delta\sigma_L$ Measurements in the pn System</u>

We are currently measuring the parameter $\Delta\sigma_L$ in pn scattering covering the momentum region of 1.0 to 3.0 GeV/c. We can investigate possible structures in I = 0 state. The results will be available within several weeks.

REFERENCES

1. R. L. Jaffee, Phys. Rev. Lett. 38, 195 (1977) and Errata 38, 617 (1977).
2. P. J. G. Mulders, A. Th. M. Aerts, and J. J. DeSwart, Phys. Rev. Lett. 40, 1543 (1978).
3. H. Lipkin, private communication.
4. I. P. Auer et al., Phys. Lett. 67B, 113 (1977).
5. I. P. Auer et al., Phys. Lett. 70B, 475 (1977).
6. I. P. Auer et al., Phys. Rev. Lett. 41, 354 (1978).
7. For $\Delta\sigma_T$ data see W. deBoer et al., Phys. Rev. Lett. 34, 558 (1975); E. K. Biegert et al., Phys. Lett. 73B, 235 (1978).
8. P. Kroll, private communication; N. Grein and P. Kroll, Nucl. Phys. B., to be published.
9. K. Hidaka et al., Phys. Lett. 70B, 479 (1977).
10. A compilation of NN and ND interactions, UCRL-20000 NN (1977).
11. To obtain the total elastic cross section from 1.2 to 1.7 GeV/c, we have integrated the differential cross-section data by B. A. Ryan et al., Phys. Rev. 3, 1 (1971). These data were used because of internal consistency.
12. M. G. Albrow et al., Nucl. Phys. B23, 445 (1970).
13. I. P. Auer et al., to be published.
14. N. Hoshizaki, paper submitted to this conference; N. Hoshizaki, Prog. Theor. Phys. 57, 1099 (1977).
15. Differential cross section data: B. A. Ryan et al., Phys. Rev. 3D, 1 (1971); D. T. Williams et al., Nuovo Cimento, 8A, 447 (1972); K. Abe et al., Phys. Rev. 12D, 1 (1975); M. G. Albrow et al., Nucl. Phys. B23, 445 (1970).
16. N. Tamura, private communication.
17. M. G. Mescheryakov, B. S. Neganov, N. P. Bogachev, and V. M. Sidorov, Dokl, Akad, Nauk SSSR 100, 673 (1955); M. G. Mescheryakov and B. S. Neganov, Kokl. Akad. Nauk SSSR 100, 677 (1955); B. S. Neganov and L. B. Parfernov, Zh. Esperrim, i Teor Fiz. 34, 767 (1958) (translation: Soviet Phys. - JETP 7, 528 (1958).

18. R. A. Arndt, Phys. Rev. 165, 1834 (1968); G. L. Kane and G. H. Thomas, Phys. Rev. D13, 2944 (1976); L. M. Libby and E. Predazz, Lettere Al Nuovo Cimento, Vol. II, N. 18, 881 (1969); J. H. Hall et al., Nucl. Phys. B12, 573 (1969); H. Suzuki, Prog. Theor. Phys. 54, 143 (1975) and earlier references therein.

19. R. A. Arndt, talk given during LAMPF Nucleon-Nucleon Workshop, July, 1978.

20. A. Beretvas et al., Rev. Mod. Phys. 39, 536 (1967); G. Colgnet et al.; J. Simmons et al.; H. Willard et al.

21. A. Lin et al., Phys. Lett. 74B, 273 (1978).

22. U. Amaldi, M. Jacob and G. Matthiae, Ann. Rev. Nucl. Sci. 26, 385 (1976).

23. D. Miller et al., Phys. Rev. Lett. 36, 763 (1976); Phys. Rev. 16D, 2016 (1977).

24. Preliminary data.

25. E. L. Berger, P. Pirila and G. H. Thomas, ANL-HEP-75-72.

26. W. M. Kloet et al., Phys. Rev. Lett. 39, 1646 (1977).

27. M. Arik and P. G. Williams, Nucl. Phys. B136, 425 (1978).

FIGURE CAPTIONS

Fig. 1 PP Total Cross Section

Fig. 2a Beam Line for the $\Delta\sigma_L$ Measurement

Fig. 2b Experimental Setup for the $C_{LL} = (L,L;0,0)$ Measurement

Fig. 3a Total Cross-Section Difference $\Delta\sigma_L = \sigma^{Tot}(\rightleftarrows) - \sigma^{Tot}(\rightrightarrows)$

Fig. 3b Total Cross Sections for Pure Initial Spin States. The dotted curves are only to guide the eye.

Fig. 4 Total Cross Section Difference, $\Delta\sigma_L$, up to 12 GeV/c

Fig. 5 $(k^2/4\pi)\ \Delta\sigma_L$ Together With $(k^2/4\pi)\ \Delta\sigma_T$

Fig. 6 Argand Plot of the $[\phi_1(0) - \phi_3(0)]$

Fig. 7 Elastic Total Cross Section

Fig. 8 Polarization at $0.1 < |t| < 0.2$

Fig. 9 Results of Legendre Coefficient Analysis

Fig. 10 $C_{LL} = (L,L;0,0)$ Data at 1.0 to 2.5 GeV/c

Fig. 11 $C_{LL} = (L,L;0,0)$ at $\theta_{c.m.} = 90^\circ$

Fig. 12a $k^2 C_{LL}(d\sigma/d\Omega)$ at $\theta_{c.m.} \approx 90^\circ$ vs. p_{lab}. The dashed curve is only to guide the eye. The solid curve is the contribution of the ${}^3F_3$ resonance over a smooth background.

Fig. 12b $k^2 C_{LL}(d\sigma/d\Omega)$ at $\theta_{c.m.} \approx 74^\circ$ vs. p_{lab}. The dashed curve is only to guide the eye.

Fig. 13 $k^2 C_{NN}(d\sigma/d\Omega)$ at $\theta_{c.m.} = 90^\circ$.

Fig. 14 Re/Im at $|t| = 0$.

Fig. 15 $(k^2/4\pi)(\Delta\sigma_T - \Delta\sigma_L)$

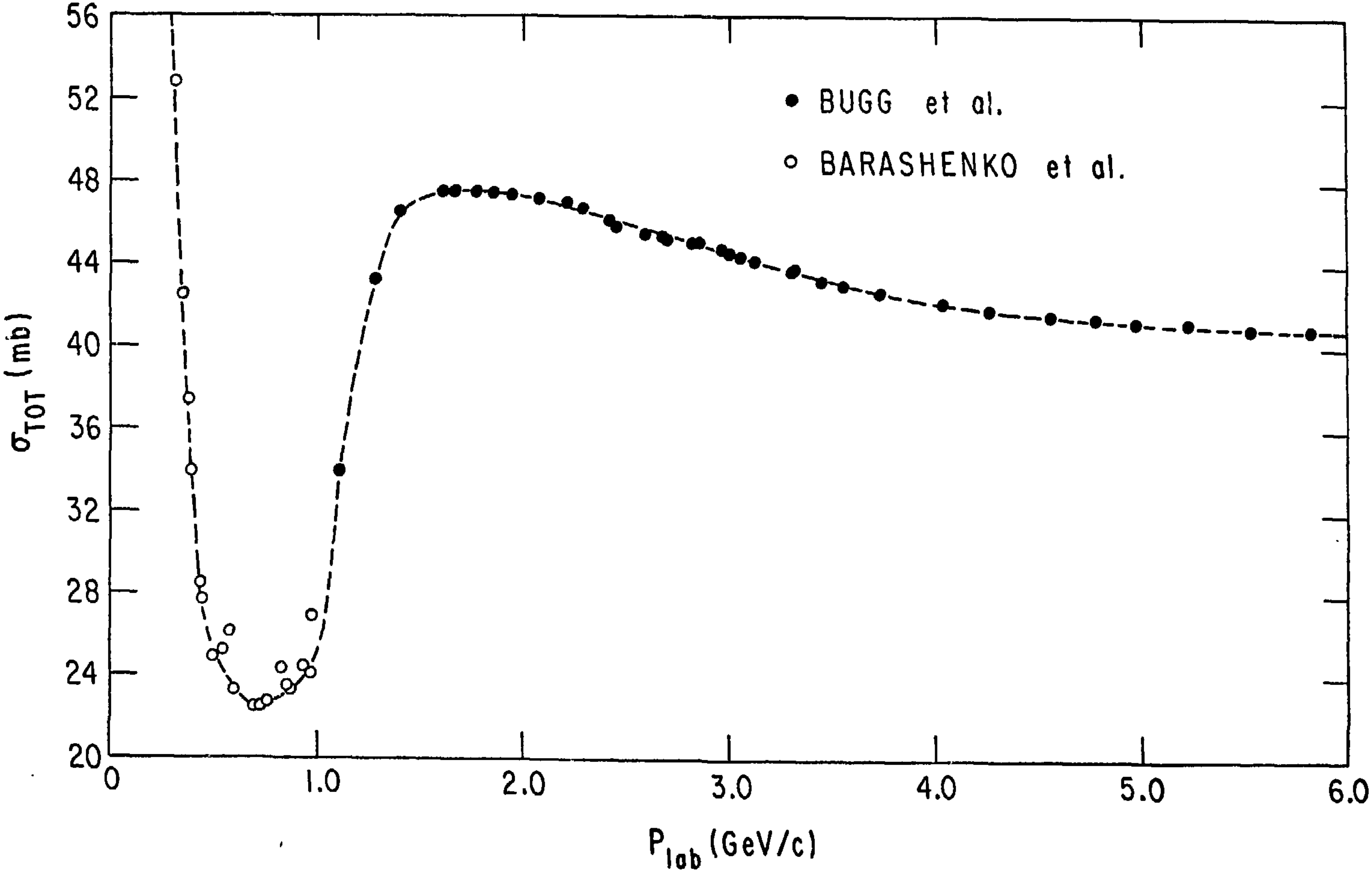

BUGG et al.
BARASHENKO et al.
σ_{TOT} (mb)
56
52
48
44
40
36
32
28
24
20
0
1.0
2.0
3.0
4.0
5.0
6.0
P_{lab} (GeV/c)

Fig. 1

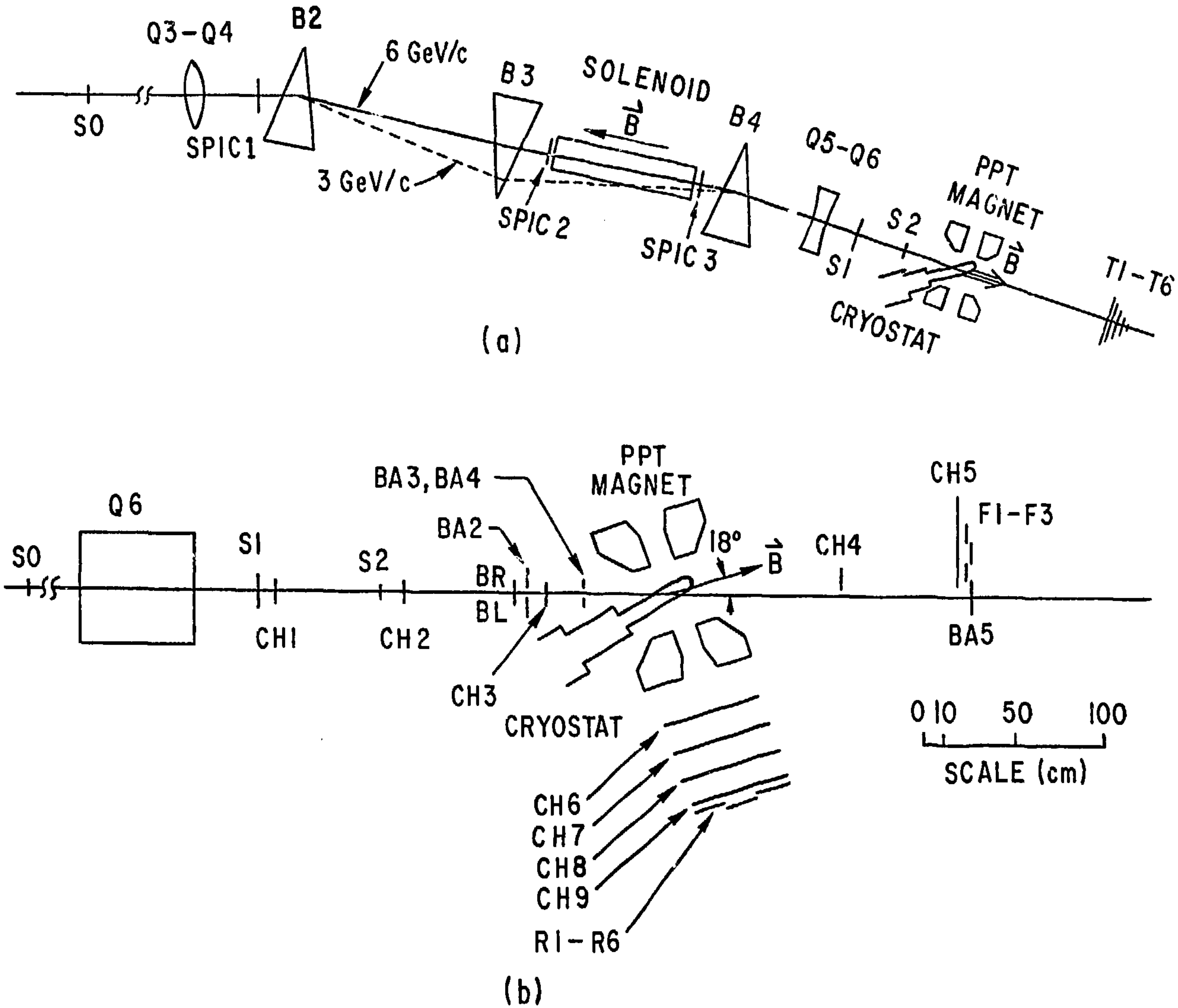
Q3-Q4
B2
6 GeV/c
B3
SOLENOID
B
B4
Q5-Q6
PPT
MAGNET
S0
SPIC1
3 GeV/c
SPIC 2
SPIC 3
S1
S2
B
T1-T6
CRYOSTAT
(a)
PPT
MAGNET
BA3, BA4
CH5
Q6
BA2
F1-F3
S0
S1
S2
18°
B
CH4
BR
BL
CH1
CH2
BA5
CH3
CRYOSTAT
0 10 50 100
SCALE (cm)
CH6
CH7
CH8
CH9
R1-R6
(b)

Fig. 2

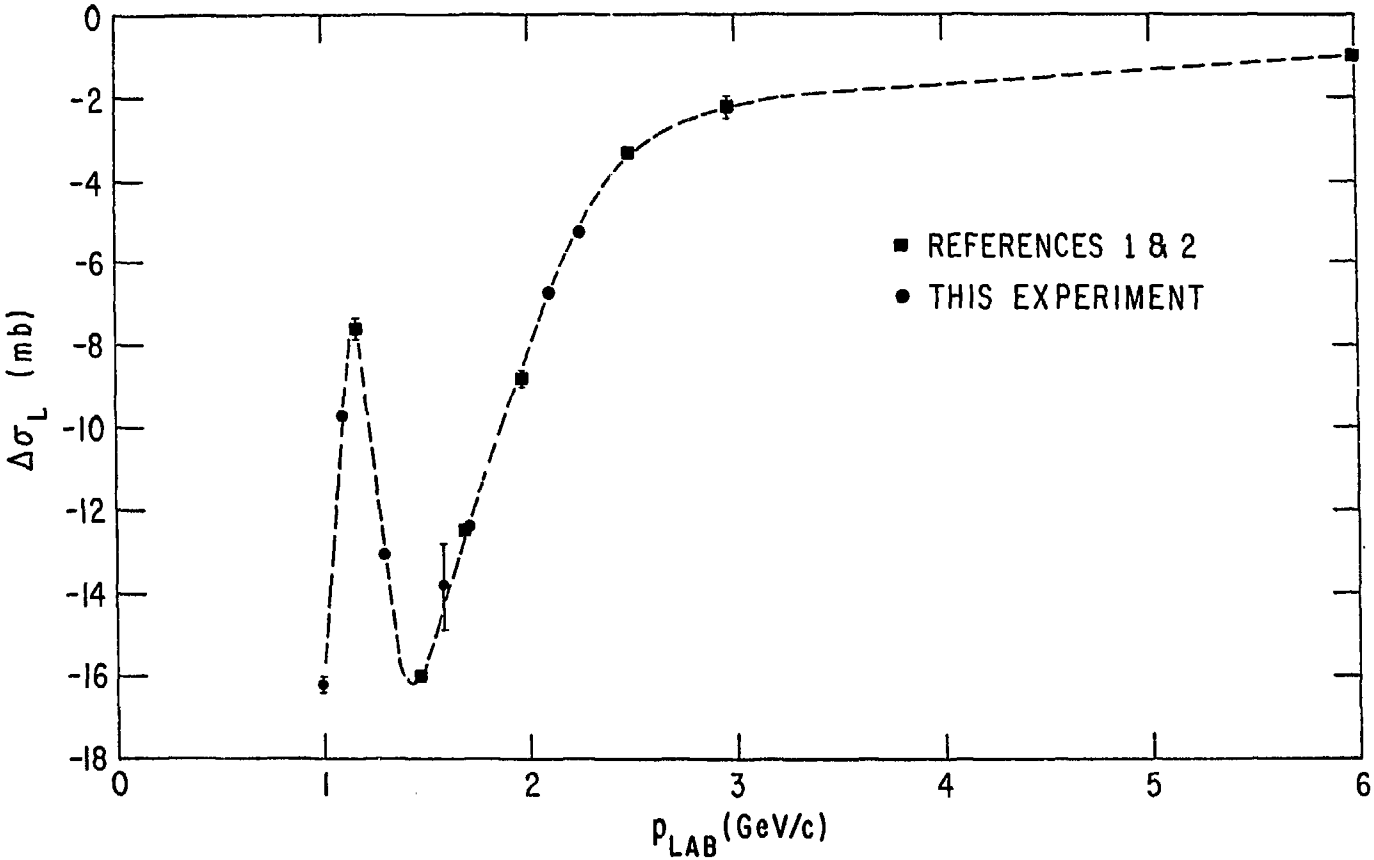

0
-2
-4
-6
-8
-10
-12
-14
-16
-18
Δσ_L (mb)
0
1
2
3
4
5
6
p_LAB (GeV/c)
REFERENCES 1 & 2
THIS EXPERIMENT

Fig. 3a

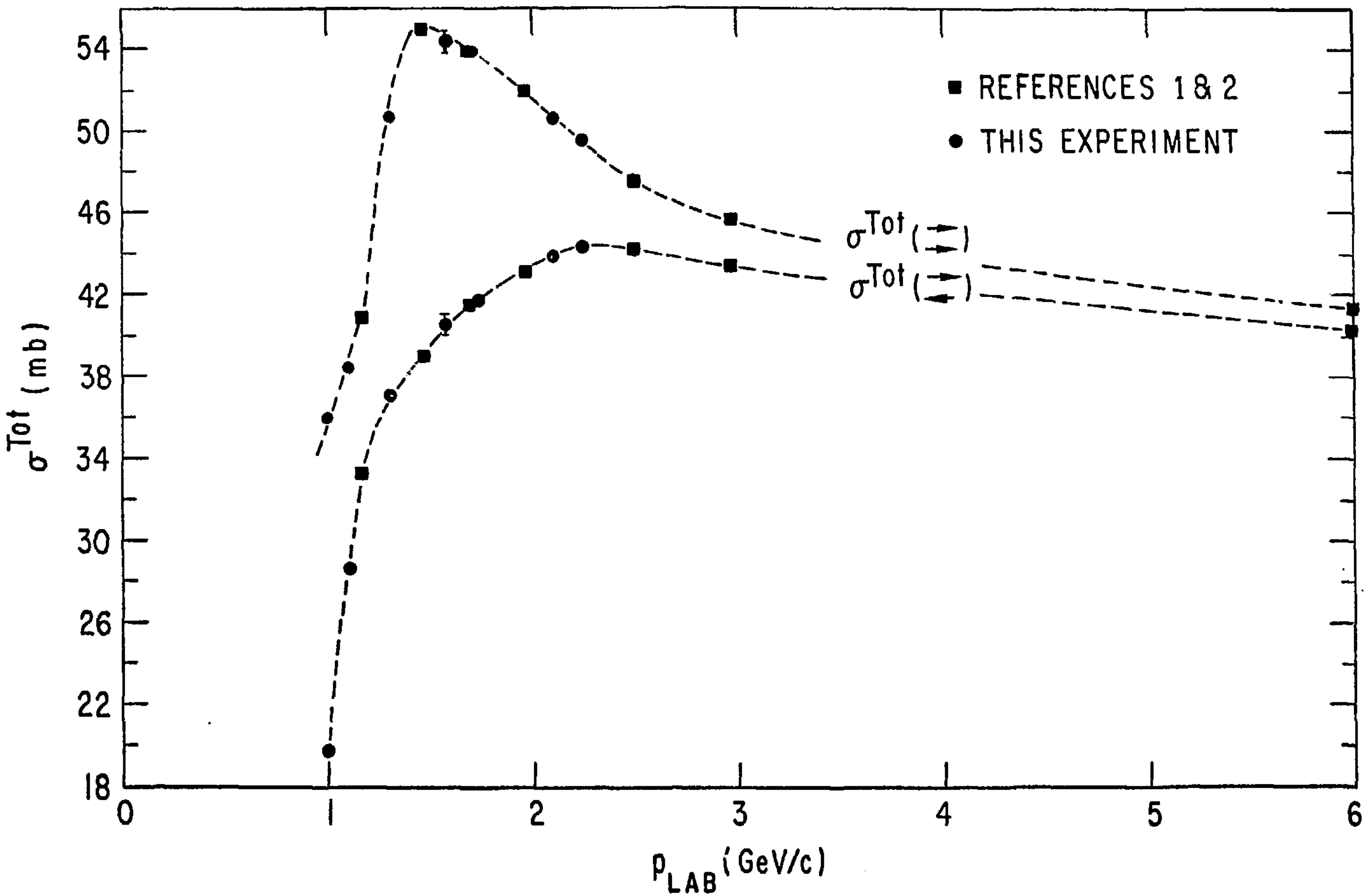

REFERENCES 1 & 2
THIS EXPERIMENT
$\sigma^{Tot}(\rightrightarrows)$
$\sigma^{Tot}(\rightleftarrows)$
σ^{Tot} (mb)
p_{LAB} (GeV/c)
54
50
46
42
38
34
30
26
22
18
0
1
2
3
4
5
6

Fig. 3b

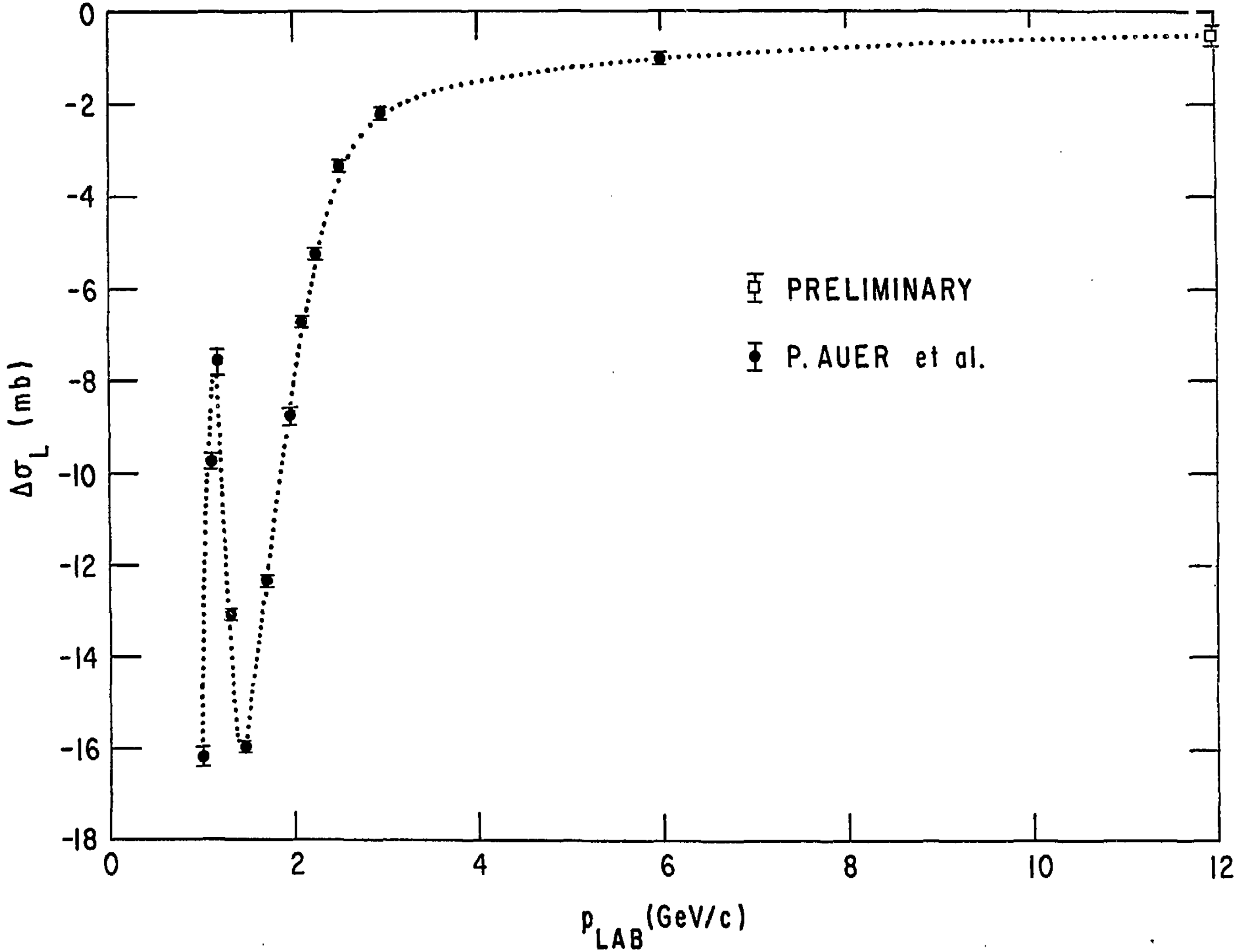

0
-2
-4
-6
-8
-10
-12
-14
-16
-18
0
2
4
6
8
10
12
PRELIMINARY
P. AUER et al.
$\Delta\sigma_L$ (mb)
p_{LAB} (GeV/c)

Fig. 4

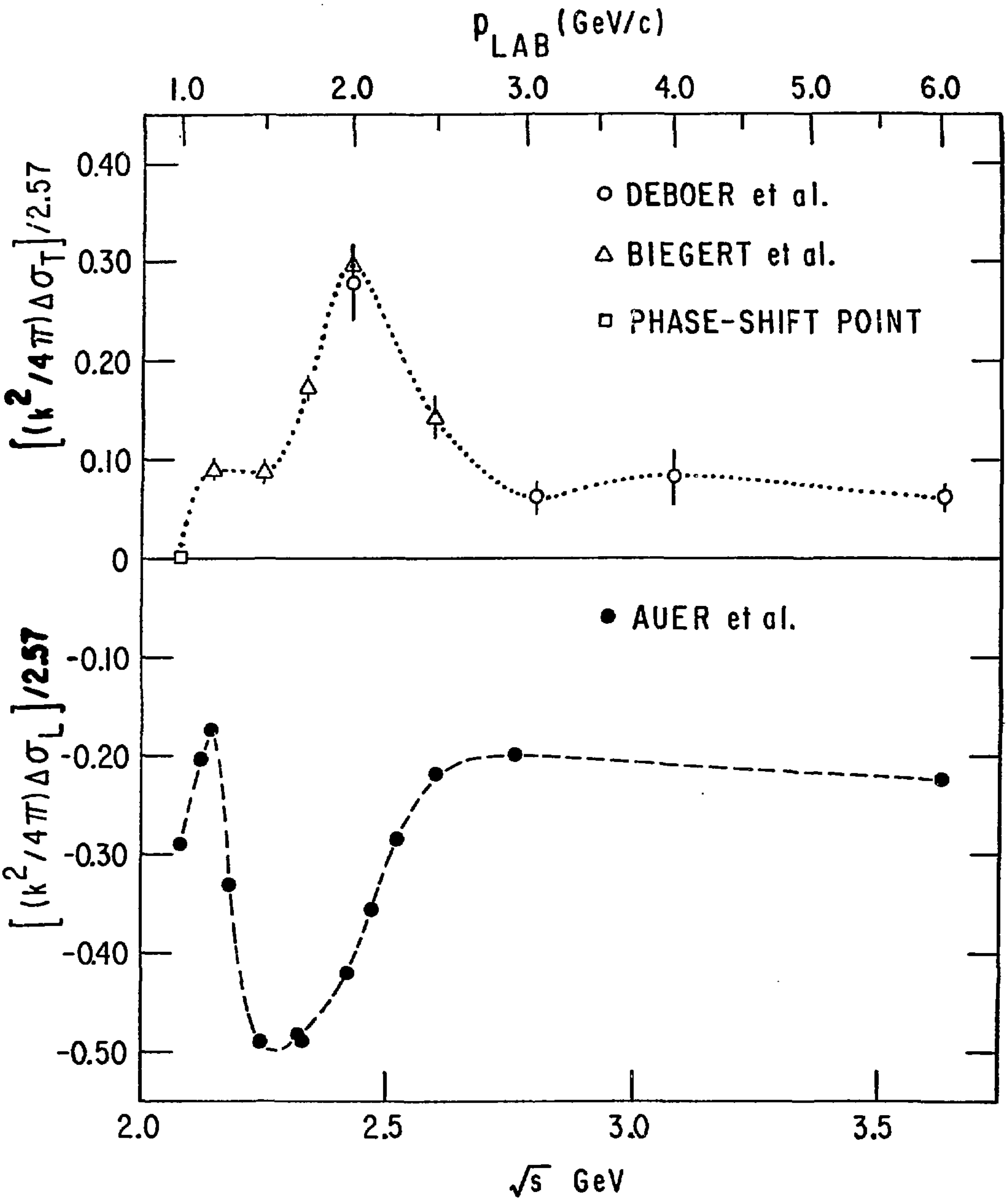

p_{LAB} (GeV/c)
1.0
2.0
3.0
4.0
5.0
6.0
0.40
0.30
0.20
0.10
0
-0.10
-0.20
-0.30
-0.40
-0.50
$[(k^2/4\pi)\Delta\sigma_T]/2.57$
$[(k^2/4\pi)\Delta\sigma_L]/2.57$
○ DEBOER et al.
△ BIEGERT et al.
□ PHASE-SHIFT POINT
● AUER et al.
2.0
2.5
3.0
3.5
$\sqrt{s}$ GeV

Fig. 5

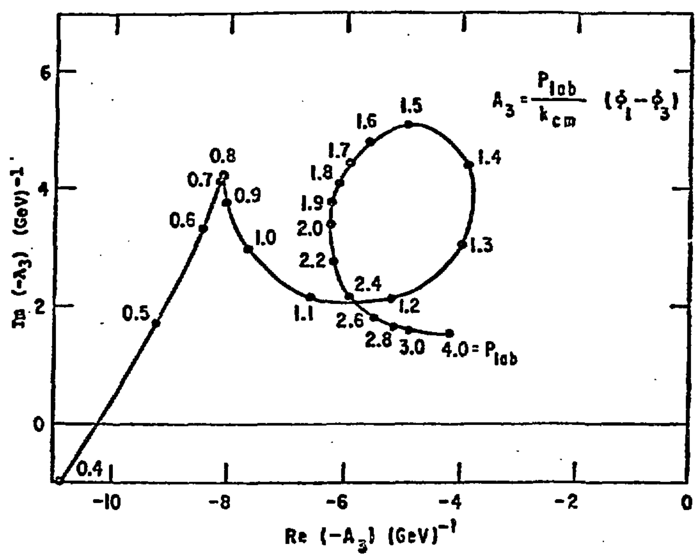

$A_3 = \frac{P_{lab}}{k_{cm}} (\phi_1 - \phi_3)$
0.4
0.5
0.6
0.7
0.8
0.9
1.0
1.1
1.2
1.3
1.4
1.5
1.6
1.7
1.8
1.9
2.0
2.2
2.4
2.6
2.8
3.0
4.0 = P_{lab}
6
4
2
0
-10
-8
-6
-4
-2
0
Im $(-A_3)$ $(GeV)^{-1}$
Re $(-A_3)$ $(GeV)^{-1}$

Fig. 6

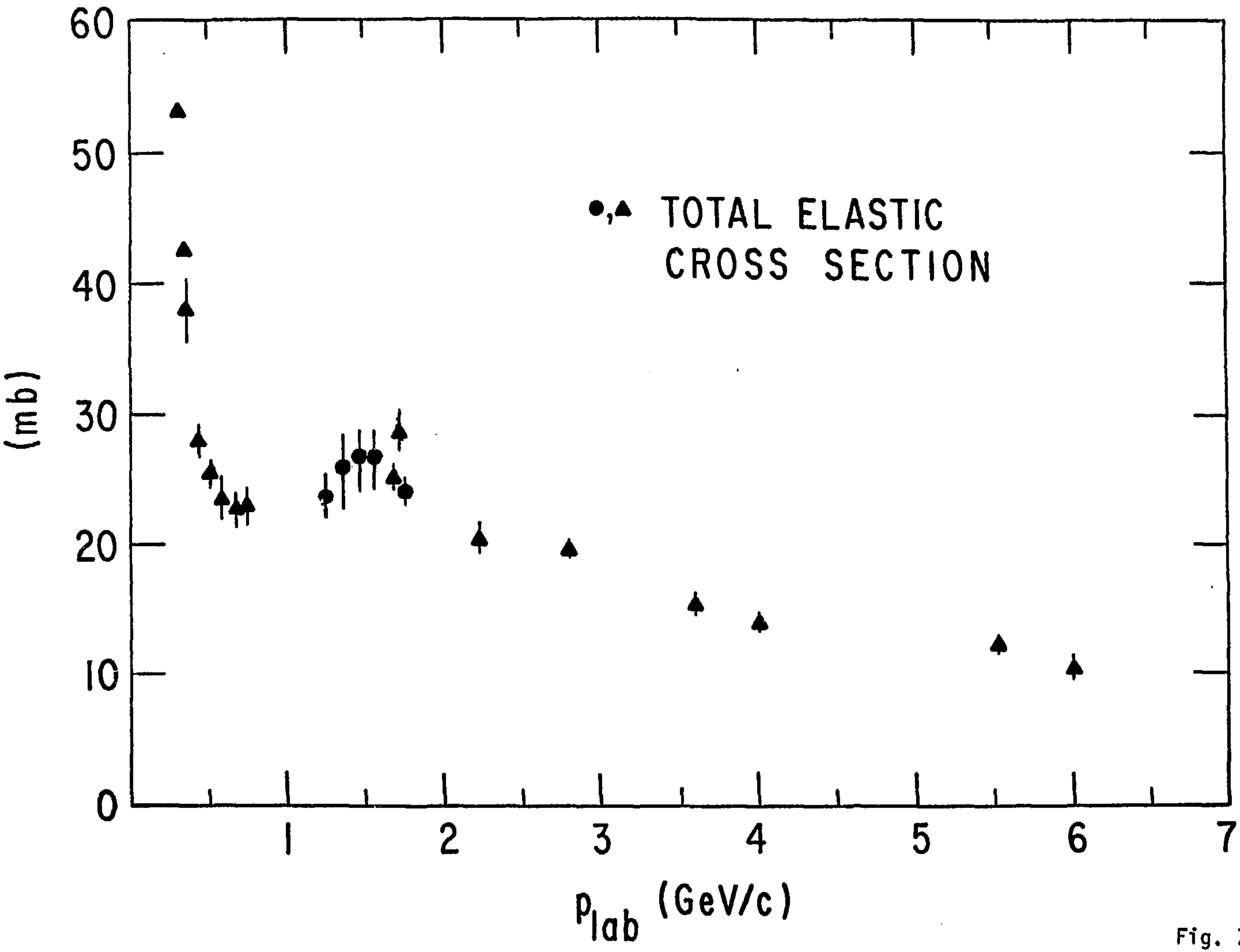

60
50
40
30
20
10
0
(mb)
●,▲ TOTAL ELASTIC
CROSS SECTION
1
2
3
4
5
6
7
p_{lab} (GeV/c)

Fig. 7

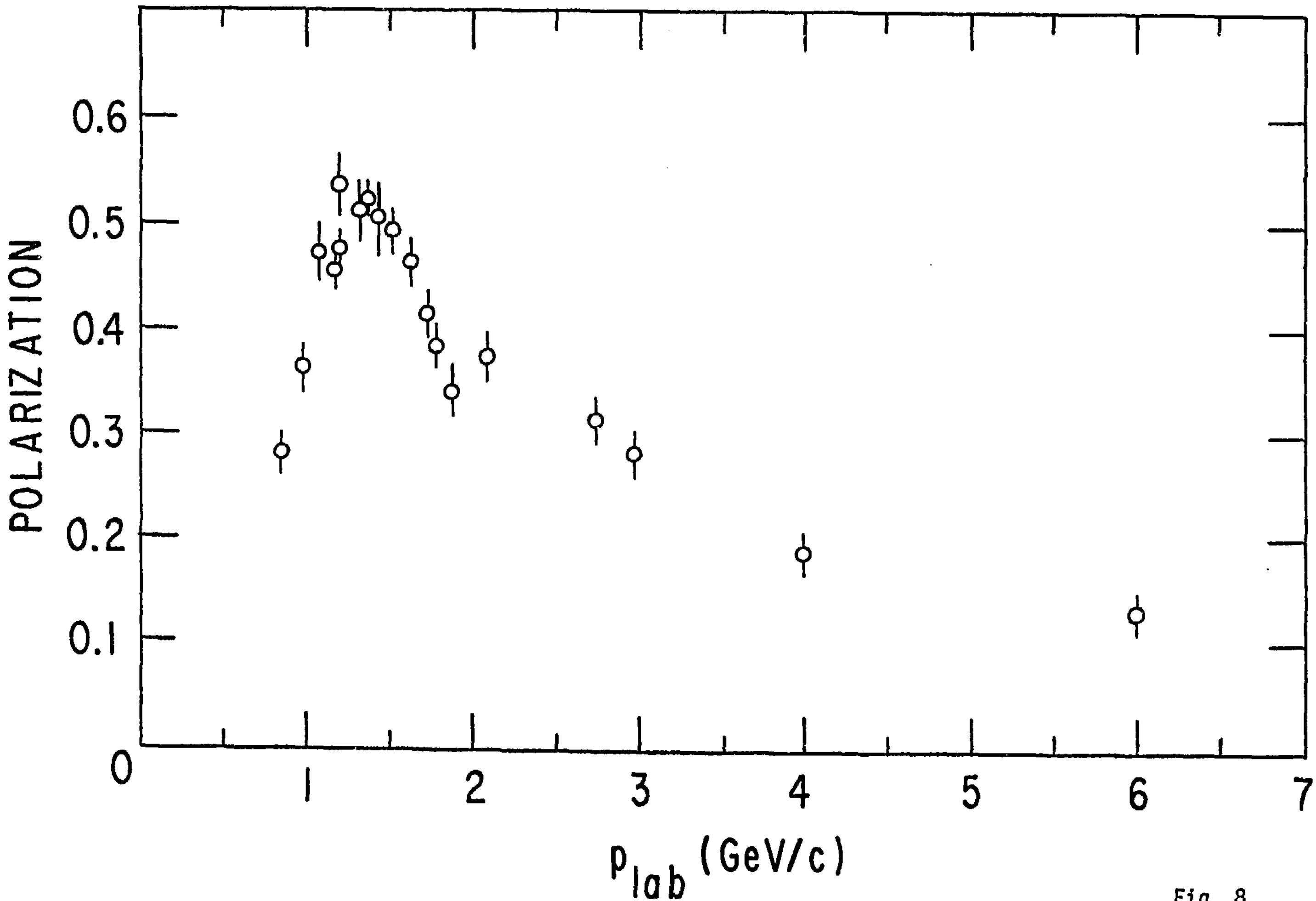

Fig. 8

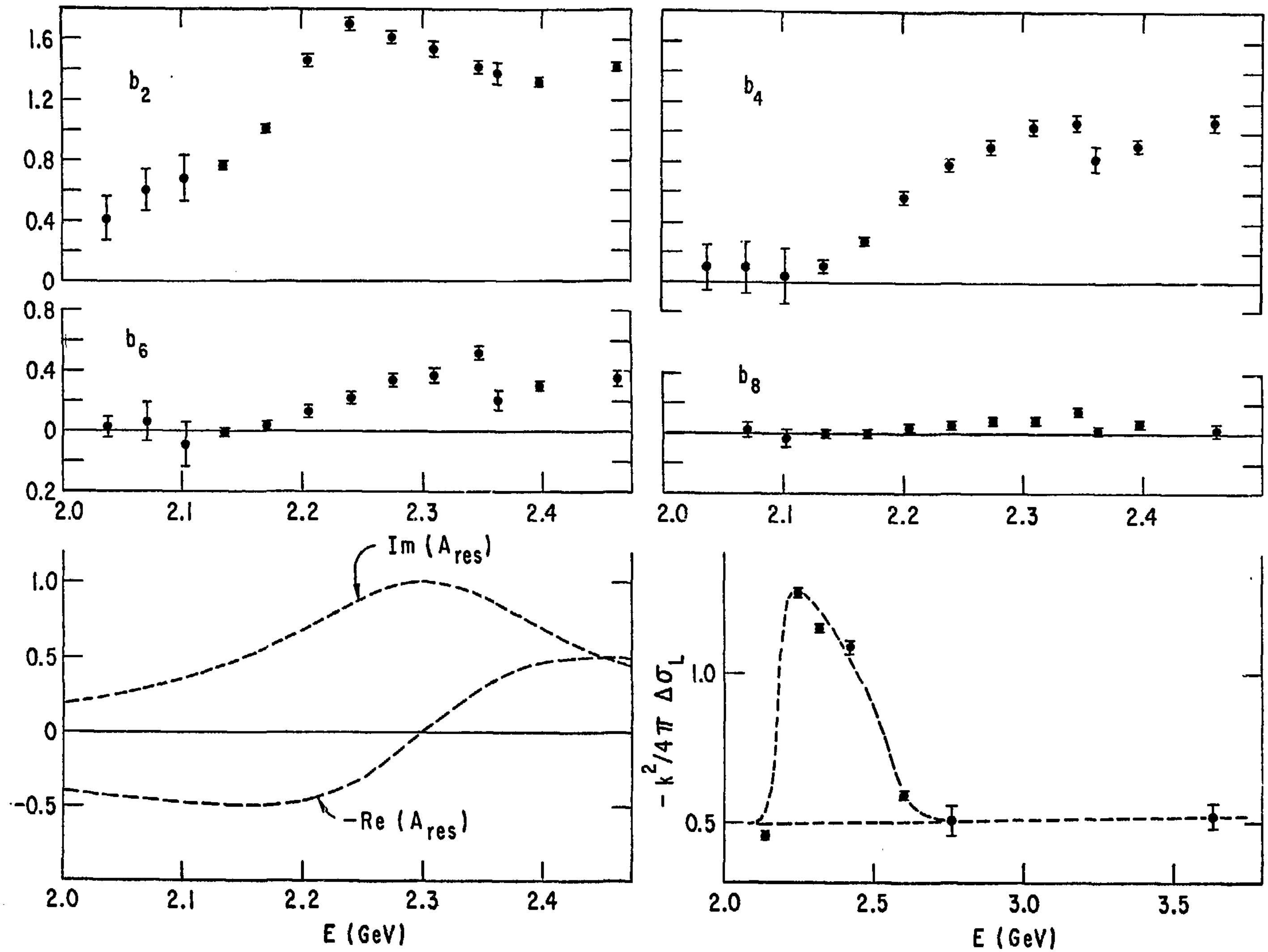

b2
b4
b6
b8
1.6
1.2
0.8
0.4
0
0.2
2.0
2.1
2.2
2.3
2.4
Im (A res)
-Re (A res)
1.0
0.5
-0.5
E (GeV)
- k²/4π Δσ L
2.5
3.0
3.5

Fig. 9

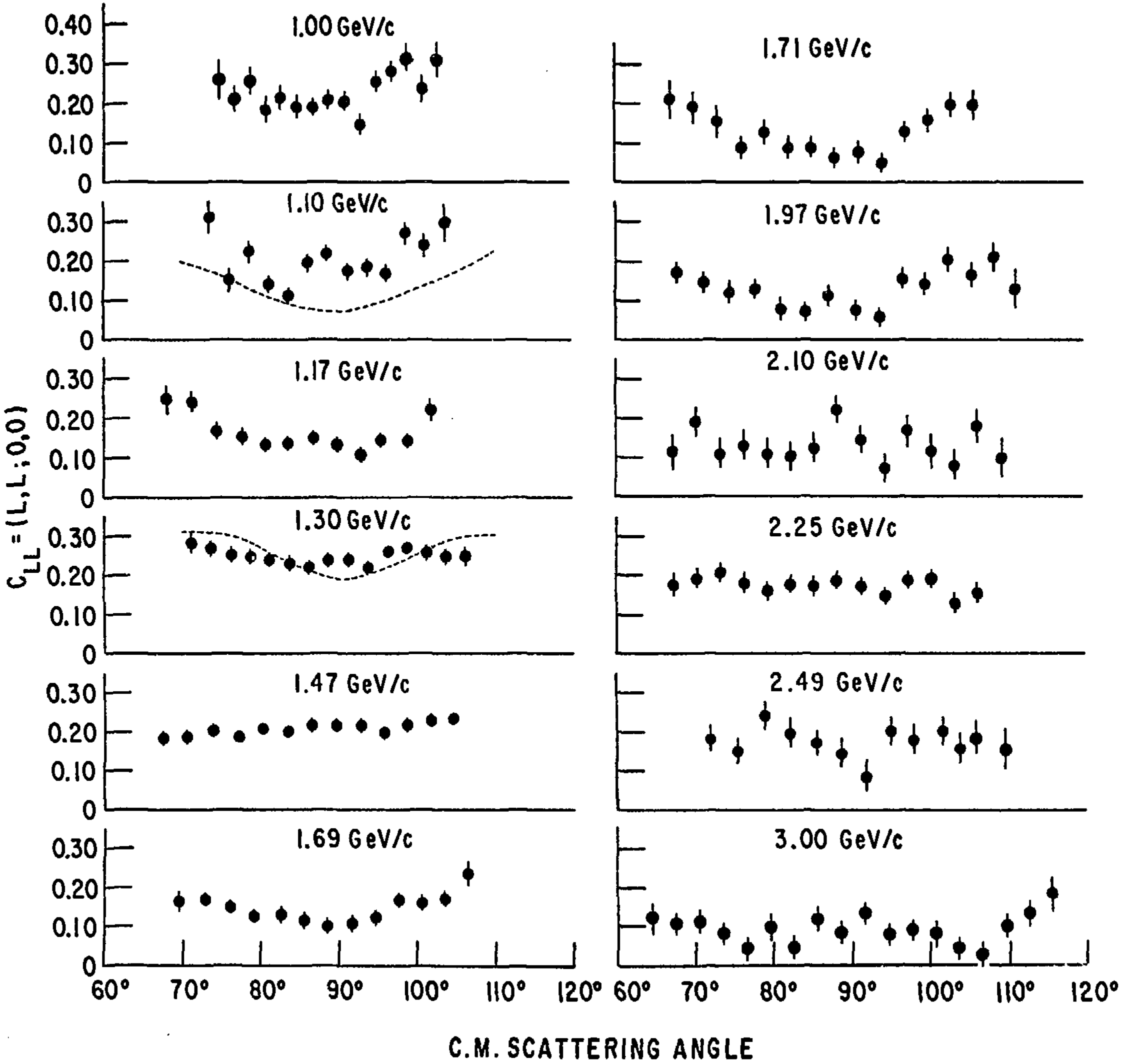
1.00 GeV/c
1.10 GeV/c
1.17 GeV/c
1.30 GeV/c
1.47 GeV/c
1.69 GeV/c
1.71 GeV/c
1.97 GeV/c
2.10 GeV/c
2.25 GeV/c
2.49 GeV/c
3.00 GeV/c
0.40
0.30
0.20
0.10
0
C_{LL}=(L,L;0,0)
60°
70°
80°
90°
100°
110°
120°
C.M. SCATTERING ANGLE

Fig. 10

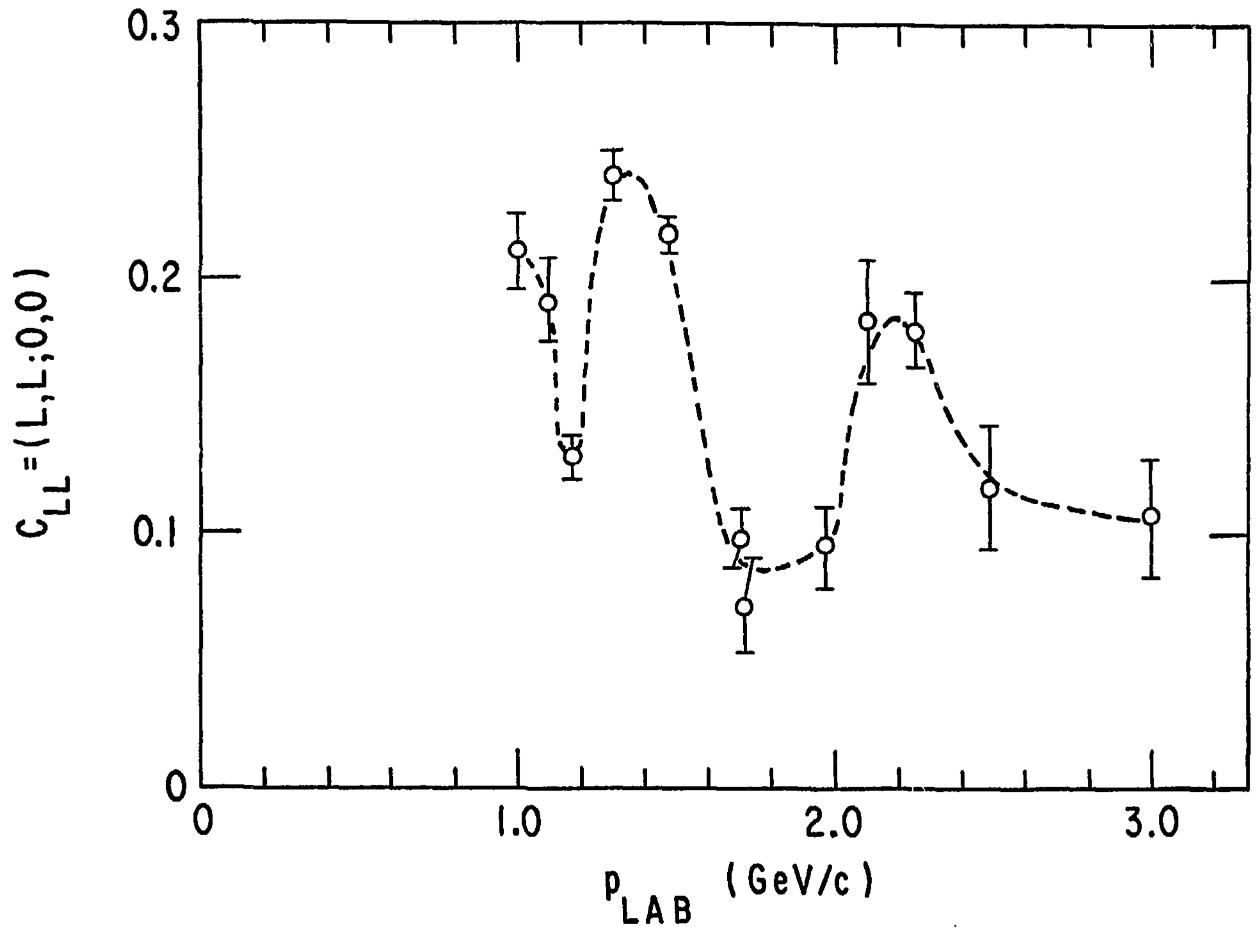

Fig. 11

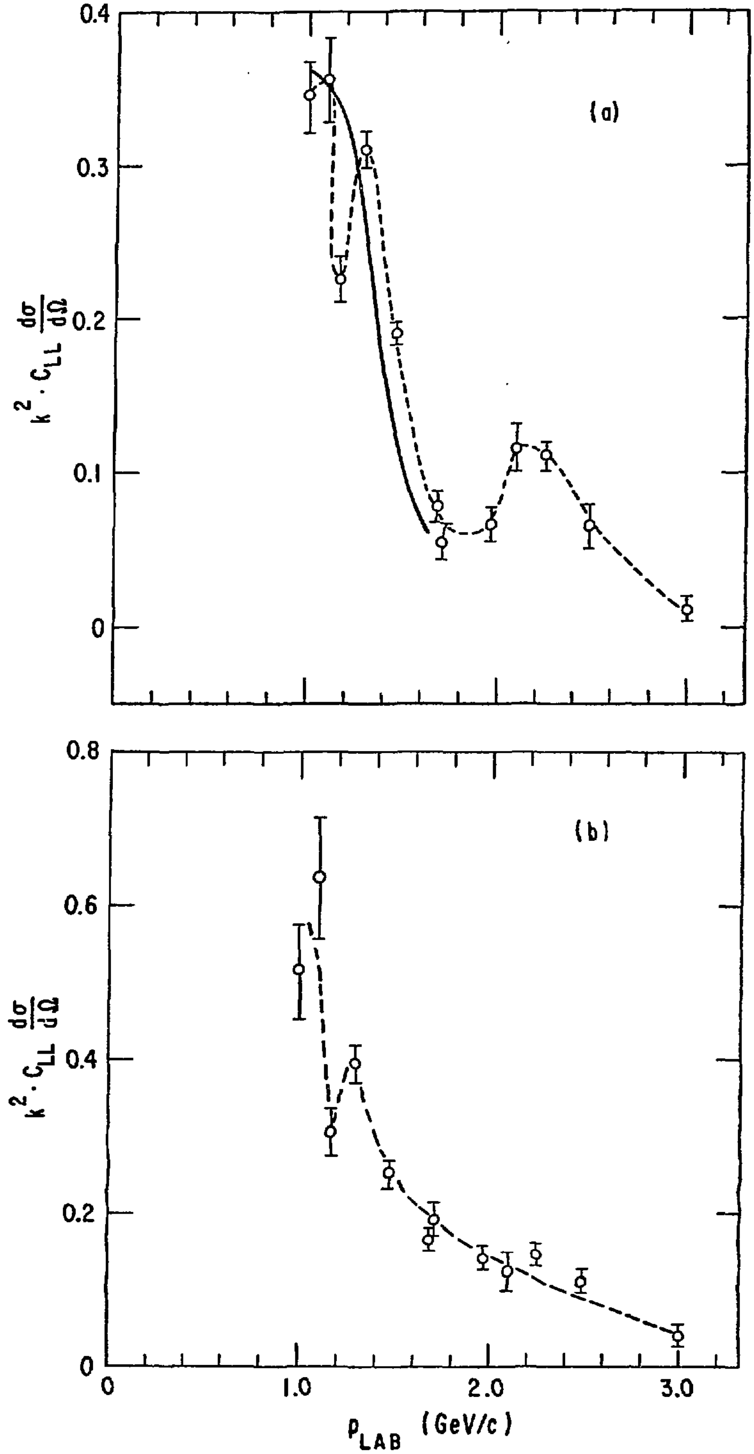

0.4
0.3
0.2
0.1
0
(a)
k² · C_LL dσ/dΩ
0.8
0.6
0.4
0.2
0
(b)
k² · C_LL dσ/dΩ
0
1.0
2.0
3.0
p_LAB (GeV/c)

Fig. 12

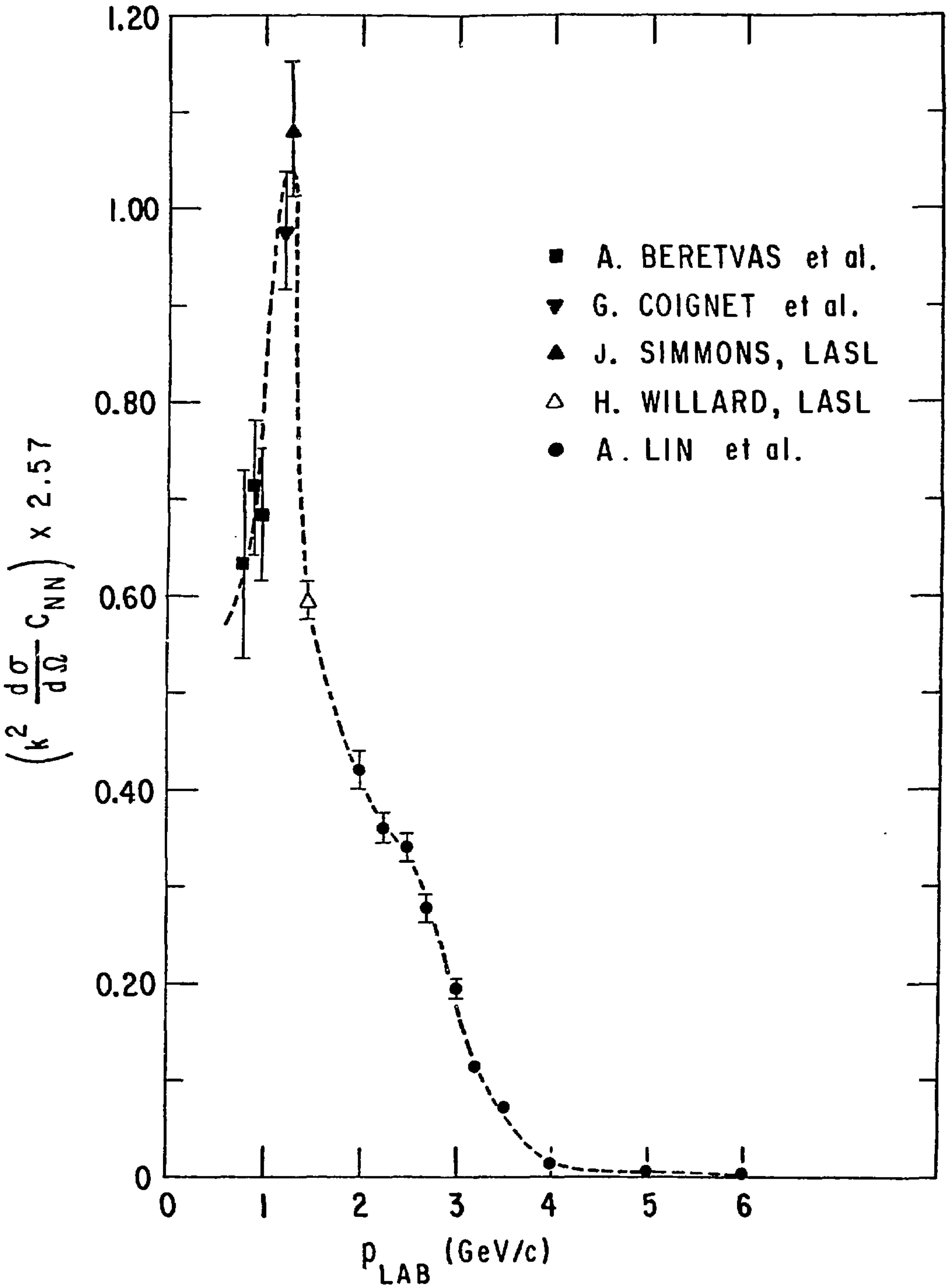
A. BERETVAS et al.
G. COIGNET et al.
J. SIMMONS, LASL
H. WILLARD, LASL
A. LIN et al.
1.20
1.00
0.80
0.60
0.40
0.20
0
0
1
2
3
4
5
6
$\left(k^2 \frac{d\sigma}{d\Omega} C_{NN}\right) \times 2.57$
p_{LAB} (GeV/c)

Fig. 13

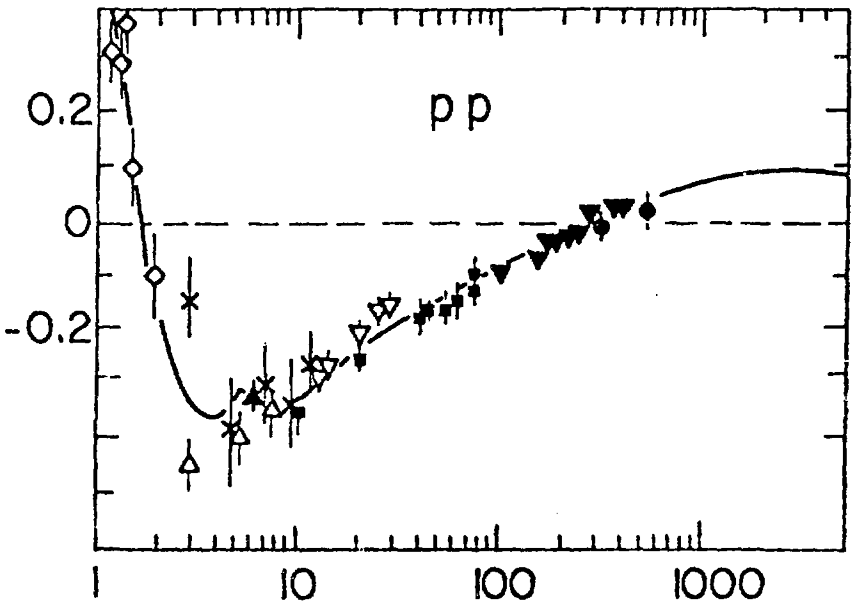

Fig. 14

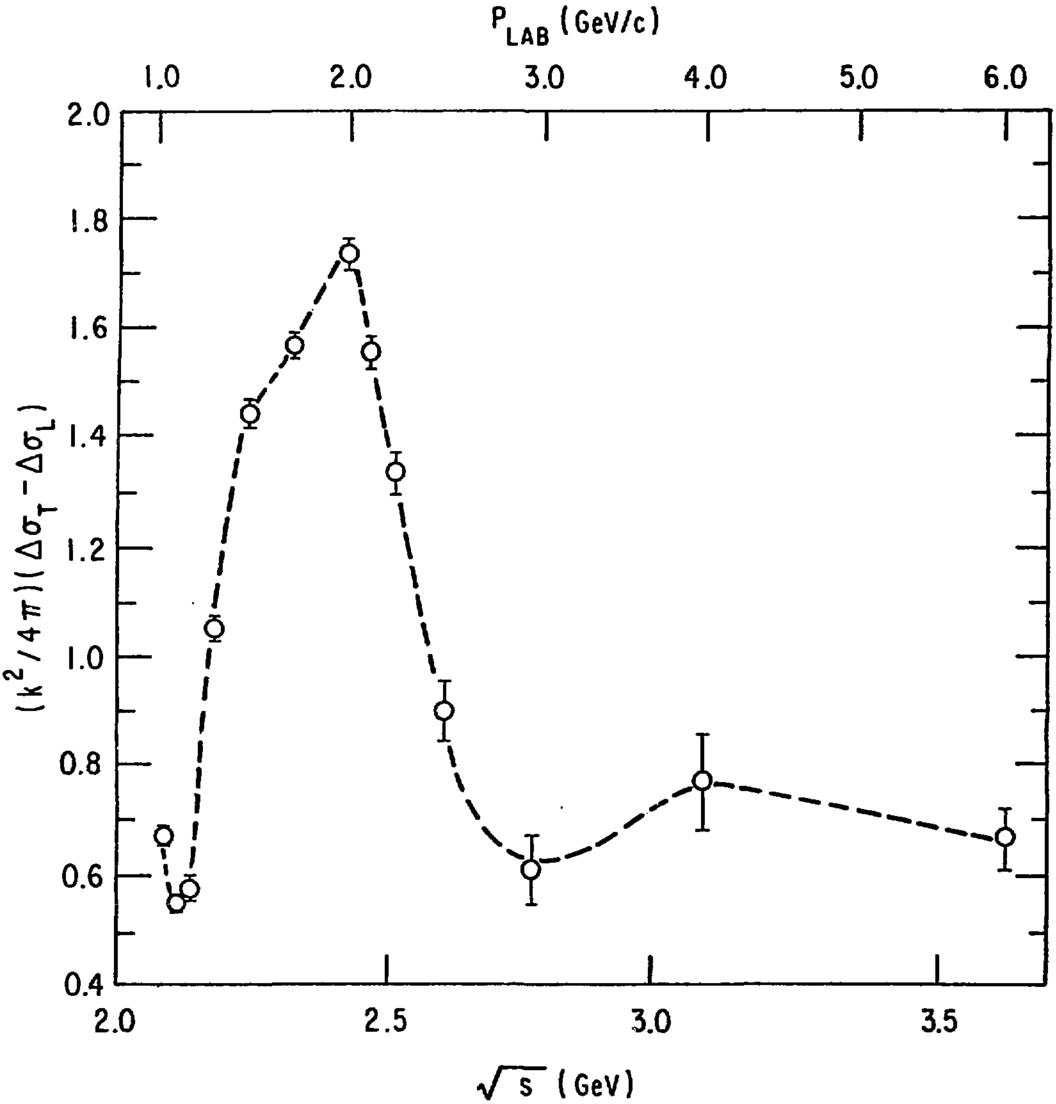

P_{LAB} (GeV/c)
1.0
2.0
3.0
4.0
5.0
6.0
2.0
1.8
1.6
1.4
1.2
1.0
0.8
0.6
0.4
$(k^2/4\pi)(\Delta\sigma_T - \Delta\sigma_L)$
2.0
2.5
3.0
3.5
$\sqrt{s}$ (GeV)

Fig. 15